ACS OMEGA

Article

Cite This: ACS Omega 2019, 4, 6154−6164

http://pubs.acs.org/journal/acsodf

Dissymmetry Factor Spectral Analysis Can Provide Useful Diastereomer Discrimination: Chiral Molecular Structure of an Analogue of (−)-Crispine A

Jordan L. Johnson,[†] Divya Sadasivan Nair,[‡] Sarath Muraleedharan Pillai,[‡] Didimos Johnson,[‡] Zabeera Kallingathodi,[‡] Ibrahim Ibnusaud,*[,‡] and Prasad L. Polavarapu*[,†]

[†]Department of Chemistry, Vanderbilt University, Nashville, Tennessee 37235, United States

[‡]Institute for Intensive Research in Basic Sciences, Mahatma Gandhi University, P.D. Hills P. O., Kottayam, Kerala 686560, India

Supporting Information

ABSTRACT: (1*R*,10*bR*)-1′-((*R*)-1,2-Dihydroxyethyl)-1-hydroxy-8,9-dimethoxy1,5,6,10*b*-tetrahydropyrrolo [2,1-*a*]-isoquinolin-3(2*H*)-one, an analogue of (−)-crispine A, with three stereogenic centers is synthesized and its absolute configuration (AC) established using the combined information derived from the synthetic scheme and single crystal X-ray diffraction data. The experimental chiroptical spectra (namely, optical rotatory dispersion (ORD), electronic circular dichroism (ECD), and vibrational circular dichroism (VCD)) and the corresponding quantum chemical (QC) predicted spectra for all diastereomers are used to evaluate the AC. The AC of the synthesized compound could be correctly established using any one of the three chiroptical spectroscopic methods (ORD, ECD, or VCD) when the relative configuration is constrained to be that derived from X-ray data or when the ACs of two of the chiral centers are constrained to be those derived from the synthetic scheme. In the absence of this outside information, the QC predicted ORD, ECD, and VCD for incorrect diastereomers are also found to satisfactorily reproduce the corresponding experimental spectra. Nevertheless, incorrect diastereomers could be eliminated when combined electronic dissymmetry factor (EDF) and vibrational dissymmetry factor (VDF) spectral analyses are included, leaving the correct diastereomer as the sole choice. Thus, the combined EDF and VDF spectral analysis is seen to be a helpful diastereomer discrimination tool.

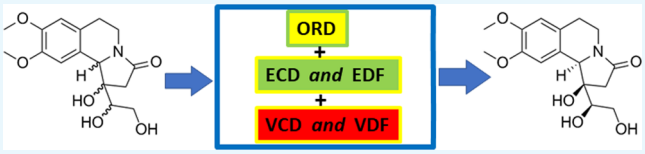

INTRODUCTION

Isoquinoline alkaloids, such as crispine A, **1**, (Figure 1), are important synthetic targets due to their potential biological activity.[1−7] (+)-**1** isolated from *Carduus crispus* L. was found to exhibit antitumor activity against certain human cancer lines.[8] The chiral solvating agents to determine the enantiomeric purity of crispine A have been investigated.[9] The enantiopure synthesis of an analogue of (−)-**1** has been reported recently using garcinia acid isolated in large amounts from tropical plant sources.[7]

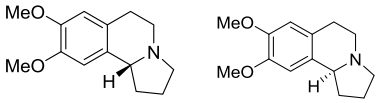

Figure 1. Structures of (+) and (−)-crispine A.

Determination of the stereostructures of chiral natural products with multiple chiral centers can be challenging. Good-quality crystals are often difficult to grow for use in single-crystal X-ray diffraction methods. In such cases, the use of NMR methods has been the widely adopted approach, although several cases are known where stereostructures were misassigned.[10−12] Chiroptical spectroscopy (optical spectroscopy suitable for studying chiral molecules) methods have become popular in recent years for the determination of absolute configurations (ACs) of chiral molecules.[13,14] Four different methods, namely, optical rotatory dispersion (ORD),[15] electronic circular dichroism (ECD),[16] vibrational circular dichroism (VCD),[17] and vibrational Raman optical activity (VROA),[18] are widely practiced under the banner of chiroptical spectroscopy. ORD is a measure of specific optical rotation (SOR) as a function of wavelength, whereas SOR itself is derived from the measured optical rotation (OR) by normalizing it with concentration (in g/cm^3) and path length (in dm). The measured OR represents the rotation of plane polarized light by chiral molecules. Circular dichroism (CD) is a measure of differential absorption of left and right circularly polarized light as a function of wavelength or wavenumber. ECD arises from electronic transitions that appear in the UV−visible spectral region, whereas VCD arises from vibrational transitions that appear in the infrared spectral region. VROA represents differential vibrational Raman scattering of right and left circularly polarized light. Each of these methods has their own specific advantages/disadvantages for interrogating the

Received: December 30, 2018
Accepted: March 20, 2019
Published: April 2, 2019

DOI: 10.1021/acsomega.8b03678
ACS Omega 2019, 4, 6154−6164

Scheme 1. Synthetic Scheme and Atom Numbering Used for Specifying the AC of 5

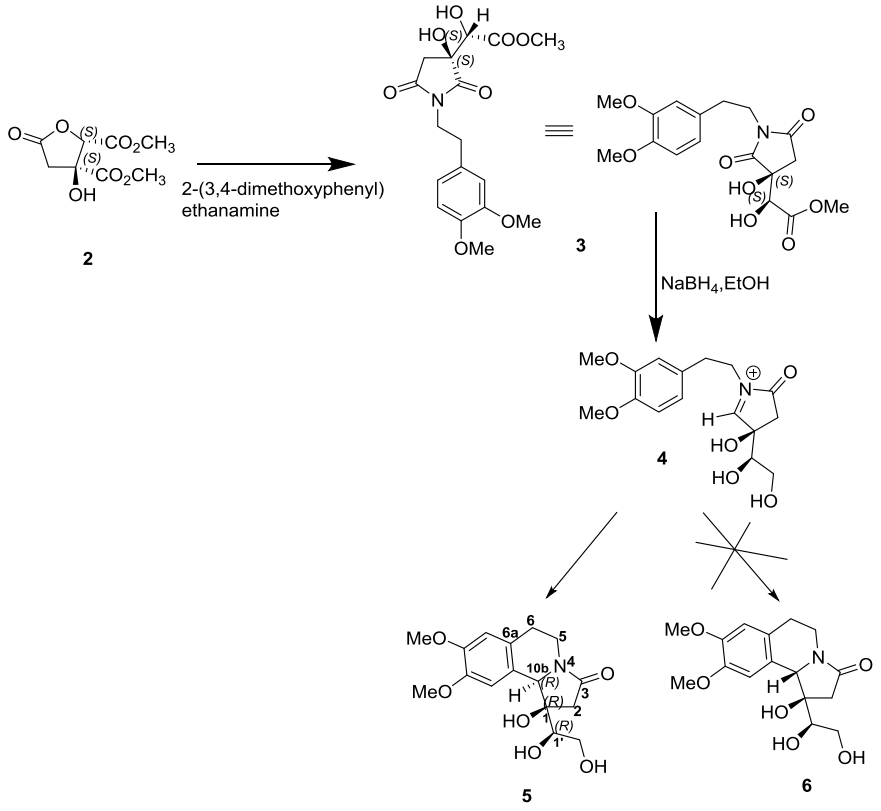

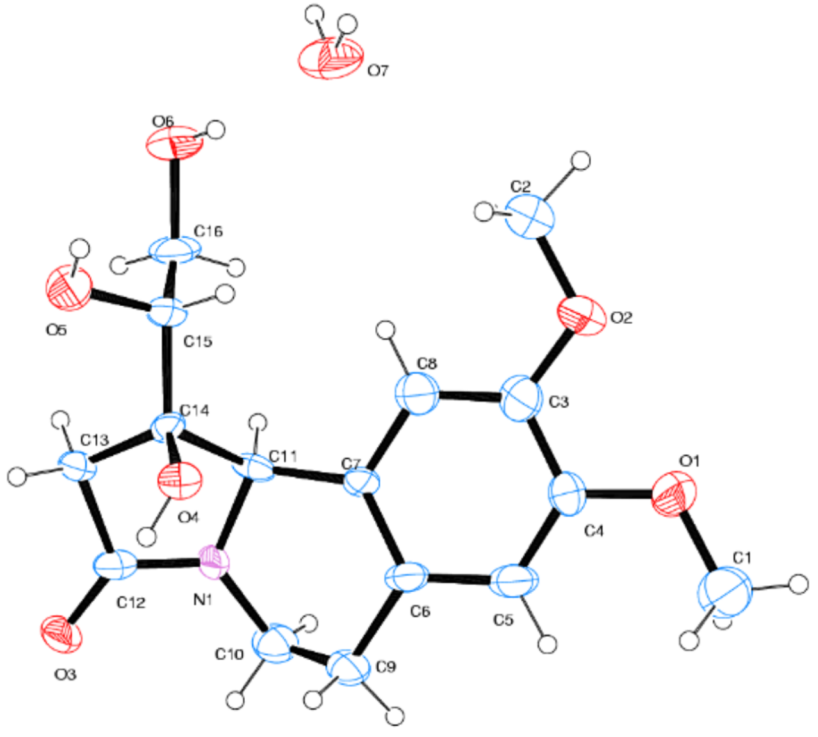

Figure 2. Crystal structure of **5**. The atom labels listed in this figure are used for summarizing the bond parameters in ESI.

chiral molecular structures, but simultaneous use of more than one method often leads to more robust structural elucidation.[19] Recent developments in quantum chemical (QC) methods[20−22] and their implementations in computer software[23−25] for predicting chiroptical spectra facilitated and popularized the analysis of experimental spectra using QC predicted spectra for deducing the chiral molecular structures.

In this manuscript, we utilize ORD, ECD, and VCD spectroscopies and X-ray crystallography for investigating the molecular structure of an analogue of (−)-**1** synthesized from

DOI: 10.1021/acsomega.8b03678
ACS Omega 2019, 4, 6154−6164

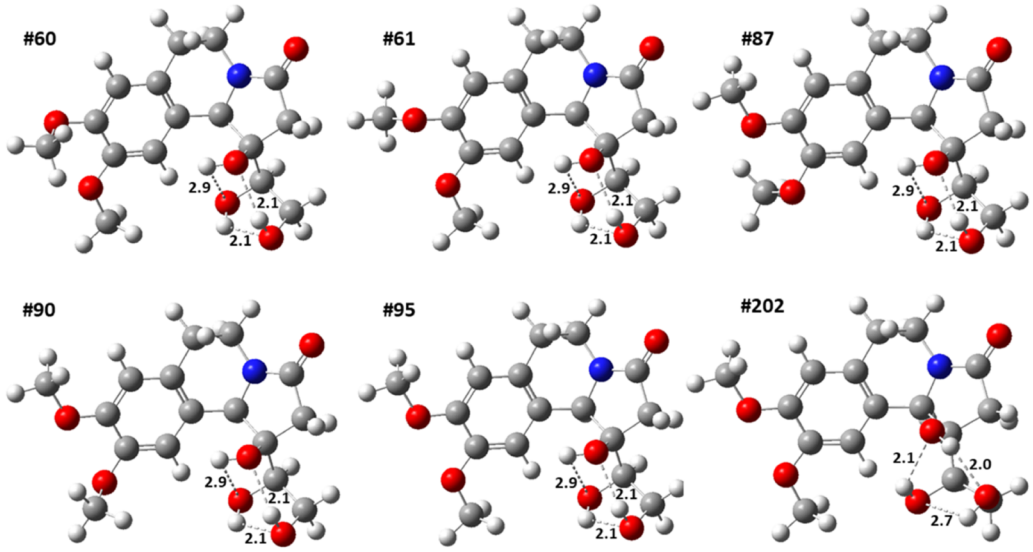

Figure 3. Six lowest energy conformers of the (1*R*,10*bR*,1′*R*) diastereomer. The intramolecular H-bonding network among the three O−H groups is depicted for each of the conformers with dashed lines, and H-bond lengths are listed in units of Å.

enantiopure (2*S*,3*S*)-dimethyl-tetrahydro-3-hydroxy-5-oxo-2,3-furandicarboxylate (garcinia ester, **2**) in two steps involving **3** and **4** (see Scheme 1). Though there are possibilities for forming two analogues of **1** from the intermediate **4**, only **5**, namely, (1*R*,10*bR*)-1′-((*R*)-1,2-dihydroxyethyl)-1-hydroxy-8,9-dimethoxy1,5,6,10*b*-tetrahydropyrrolo [2,1-a]isoquinolin-3(2*H*)-one, is obtained. The absolute configurations (ACs) at the three stereogenic centers of **5** are deduced from the synthetic scheme, and the relative configurations determined from the X-ray structure. To evaluate the capabilities of chiroptical spectroscopic methods for independently establishing the AC, the experimental ORD, ECD, and VCD spectra of **5** are also analyzed using the corresponding QC predicted spectra for all possible diastereomers.

RESULTS AND DISCUSSION

AC of 5. The procedure for chemical synthesis of **5** has been reported before.[7] Specifically (see Scheme 1), garcinia acid ester ((2*S*,3*S*)-3-hydroxy-5-oxotetrahydrofuran-2,3-dicarboxylate), **2**, was first reacted with (3,4-dimethoxyphenyl)-ethanamine to generate (*S*)-methyl 2-((*S*)-1-(3,4-dimethoxyphenethyl)-3-hydroxy-2,5-dioxopyrrolidin-3-yl)-2-hydroxyacetate, **3**. During this transformation, the ACs at chiral carbon atoms remain the same. In the subsequent step, there are possibilities for forming **5** and **6** from **3**. The key synthetic step involved here is the cyclization of the *N*-acyliminium ion, **4** (Scheme 1).[26−28] The use of $NaBH_4$ results in the formation of **5** exclusively. Conversion of **3** to **5**, via intermediate **4**, occurs without altering the stereochemistry. Therefore, it is logical to conclude that the ACs of the chiral carbon atoms 1 and 1′ are (*R*). However, a new chiral center is formed at position 10*b*, whose AC was suggested[7] using two-dimensional NMR correlations to be *R*. An independent verification of this assignment is needed. For this purpose, single-crystal X-ray diffraction measurements are undertaken to determine the relative configurations at positions 10*b*, 1, and 1′. The crystal structure of **5** is shown in Figure 2, which indicates that positions 10*b*, 1, and 1′ should all have the same stereodescriptors under Cahn−Ingold−Prelog sequence rules.[29] Therefore, the AC of **5** should be either (1*R*,10*bR*,1′*R*) or (1*S*,10*bS*,1′*S*). Since the ACs at 1 and 1′ positions are known from the synthetic scheme to be *R*, the AC of **5** is (1*R*,10*bR*,1′*R*), as depicted in Scheme 1, and is in agreement with that derived from two-dimensional NMR correlations.[7]

The crystal data, collection parameters, and refinement conditions are listed in Table S1 of the Supporting Information (SI). The selected bond lengths and bond angles are summarized in Table S2 of SI.

Chiroptical Spectroscopic Analysis of the (1*R*,10*bR*,1′*R*) Diastereomer. The details of experimental methods and spectral similarity overlap (SSO) analysis are given in the Methods section.

Conformational Analysis and Spectral Predictions. The structure of **5** with (*R*)-configuration at each of the three chiral centers was manually built and used as input for conformational search using the CONFLEX program.[30] The geometries of 1730 unique conformers generated by CONFLEX were optimized using the B3LYP functional[31−33] and the 6-31G* basis set[34] as implemented in the Gaussian 09 program.[35] This process led to 1236 optimized structures within an energy spread of 19.2 kcal/mol. Of these, the six lowest energy structures account for 97% of the population. The geometries of these six lowest energy conformers were further optimized using the polarizable continuum model (PCM)[36] for representing methanol solvent at the CAM[37]-B3LYP/6-311++G(2d,2p)/PCM level and the resulting structures used for ECD and ORD calculations at the same level. ECD and ORD calculations were also undertaken for all diastereomers using empirical D3 dispersion corrections.[38] No significant differences could be found between the results obtained with and without dispersion corrections. For VCD calculations, geometry optimizations and QC predictions of VCD were undertaken at the B3PW91/6-311++G(2d,2p)/PCM level. To account for deuterium exchange in the CD_3OD solvent that was used for experimental VCD measurements, the O−H groups of **5** were converted to O-D for VCD calculations. For (1*R*,10*bR*,1′*R*) and (1*R*,10*bS*,1′*R*) diastereomers, full geometry optimizations and VCD calculations were also carried out including empirical D3 dispersion corrections, but the inclusion of dispersion corrections did not provide improve-

DOI: 10.1021/acsomega.8b03678
ACS Omega 2019, 4, 6154−6164

Table 1. Energies, Populations[a], and Ring Puckering Angles[b] of the (1*R*,10*bR*, 1′*R*) Diastereomer with Deuterated OH Groups at B3PW91/6-311++G(2d,2p)/PCM(Methanol)

conformer	Gibbs energy	energy (kcal/mol)	population	N4−C5−C6−C6a	C1−C2−C3−N4
95	−1128.0708	0.00	0.86	−49.9	−13.5
90	−1128.068	1.77	0.04	−50.4	−13.9
202	−1128.0679	1.85	0.04	−54.1	−21.0
87	−1128.0676	2.01	0.03	−50.1	−13.7
60	−1128.0675	2.11	0.02	−49.8	−12.7
61	−1128.067	2.39	0.01	−50.1	−12.7

[a]Inclusion of empirical D3 dispersion corrections changes the listed populations to 0.76, 0.06, 0.06, 0.04, 0.04, and 0.04 in the order listed. [b]The N4−C5−C6−C6a and C1−C2−C3−N4 ring puckering angles in the crystal structure are −52.2 and −22.6, respectively.

ment over those without dispersion corrections. All ECD and VCD calculations were also undertaken using the Gaussian 09 program.[35]

There are no significant differences in the populations generated from electronic energies (at CAM-B3LYP/6-311++G(2d,2p)/PCM(methanol)) and Gibbs free energies (at B3PW91/6-311++G(2d,2p)/PCM(methanol)). The six lowest energy conformers of the (1*R*,10*bR*,1′*R*) diastereomer are displayed in Figure 3. In these conformers, O−H groups are seen to be oriented for favorable intramolecular O−H···O−H hydrogen-bonding network. The relative orientations of O−CH_3 groups differ among these conformers. The lowest energy conformer (#95) with ∼86% population has the methoxy groups turned away from each other, as also seen in the crystal structure; however, unlike in the crystal structure that has cocrystallized water molecules, the hydroxyl groups in the isolated molecule adopt an intramolecular hydrogen-bonding network as shown in Figure 3.

Table 1 reports the Gibbs energies, populations, and ring puckering angles for these six lowest energy conformers. All conformers have nearly the same ring puckering angles. Conformers with ring puckering angles opposite to the ones listed in Table 1 have higher energies and are not expected to be populated at room temperature. The lowest energy conformer (#95) is expected to be dominant with ∼86% population.

The predicted SORs for **5** are generated as a sum of those of all six conformers with individual conformer specific rotations weighted by its population. Similarly, predicted VA, VCD, EA, and ECD spectral intensities for **5** are generated as a sum of those of all six conformers with individual conformer spectral intensities weighted by its population.

ORD of the (1R,10bR,1′R) Diastereomer. The experimental SORs measured at six different wavelengths are compared to those predicted at the CAM-B3LYP/6-311++G(2d,2p)/PCM-(methanol) level in Figure 4. The signs, as well as magnitudes, of the predicted SORs for the (1*R*,10*bR*,1′*R*) diastereomer match those observed in the experiment quite well. The excellent agreement between experimental and QC predicted ORD supports the assigned AC, (1*R*,10*bR*,1′*R*), as well as the predominant conformation listed in Table 1. However, it should be noted that since methanol solvent can hydrogen bond to **5**, the predominant conformer of **5** in methanol solution can very well be different from that predicted for an isolated molecule using PCM and that difference may not be transparent from the predicted ORD.

ECD of the (1R,10bR,1′R) Diastereomer. The experimental electronic absorption (EA), ECD, and electronic dissymmetry factor (EDF) spectra are compared to the corresponding spectra for the (1*R*,10*bR*,1′*R*) diastereomer in Figure 5. Since a

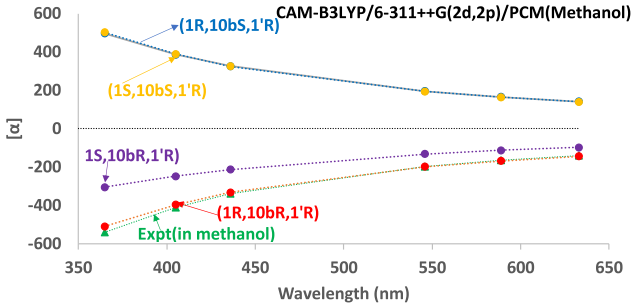

Figure 4. Comparison of experimental wavelength-dependent specific rotations with those predicted for four diastereomers of **5** at the CAM-B3LYP/6-311++G(2d,2p)/PCM(methanol) level. Inclusion of empirical D3 dispersion corrections did not influence these results.

single conformer (#95) of the (1*R*,10*bR*,1′*R*) diastereomer has the majority of the population (see Table 1), the Boltzmann-weighted EA and ECD spectra are dominated by those of this conformer. The predicted EA and ECD spectra for individual conformers and their comparison to population-weighted spectra are given in Figure S1 of the SI. In Figure 5, the left vertical panel displays the predicted spectra with wavelengths scaled by 1.02 (which corresponds to the maximum *Sim*ECD value) and overlaid on experimental spectra. In the right vertical panel, QC predicted spectra obtained with unscaled band positions are presented. The EA spectrum of **5** in the 180 and 300 nm regions measured in methanol reveals three bands: a stronger intensity band at 207, a weaker intensity band at 233, and a weak-intensity broad band at 286 nm. The QC predicted EA spectrum for the (1*R*,10*bR*,1′*R*) diastereomer at the CAM-B3LYP/6-311++G(2d,2p) level similarly shows three bands at 194, 225, and 253 nm. The experimentally measured ECD spectrum for **5** shows four bands at 203, 216, 229, and 242 nm associated with negative, positive, negative, and positive signs, respectively. The negative (229 nm) and positive (242 nm) bisignate couplet appears to be associated with the experimental 233 nm absorption band. The CAM-B3LYP/6-311++G(2d,2p)/PCM(methanol) predicted ECD spectrum reveals only three bands with a sign pattern of negative, positive, and positive at 200, 226, and 252 nm, respectively. The experimental negative cotton effect (CE) at 229 nm is not reproduced in the QC predicted spectrum, resulting in the correlation of the experimental (with predicted) ECD spectrum as follows: 200 (203), 216 (226), and 242(252) nm. Based on the predicted EA and ECD spectra, the electronic transitions observed in the experimental spectrum are considered to arise from those in the benzene ring. The molecular orbitals identifying the electronic

DOI: 10.1021/acsomega.8b03678
ACS Omega 2019, 4, 6154−6164

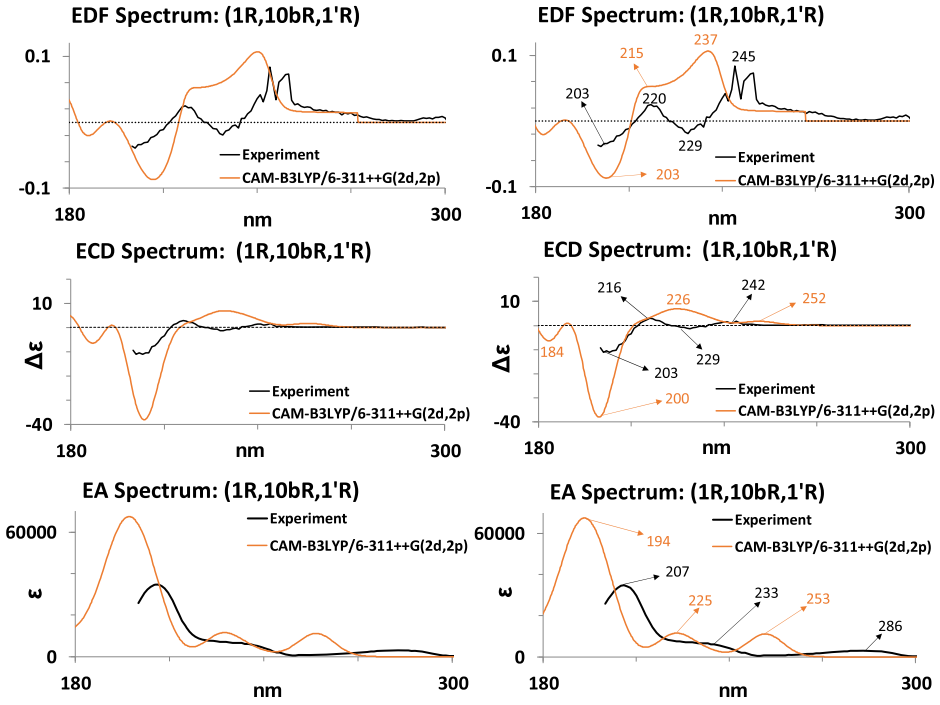

Figure 5. Comparison of experimental EA, ECD, and EDF spectra with those predicted for the (1*R*,10*bR*,1′*R*) diastereomer at CAM-B3LYP/6-311++G(2d,2p)/PCM(methanol). In the left vertical panel, the predicted wavelengths are scaled with 1.02 (which corresponds to maximum *Sim*ECD) and overlaid on experimental spectra. In the right vertical panel, QC predicted spectra obtained with unscaled band positions are presented. Inclusion of empirical D3 dispersion corrections did not influence these results.

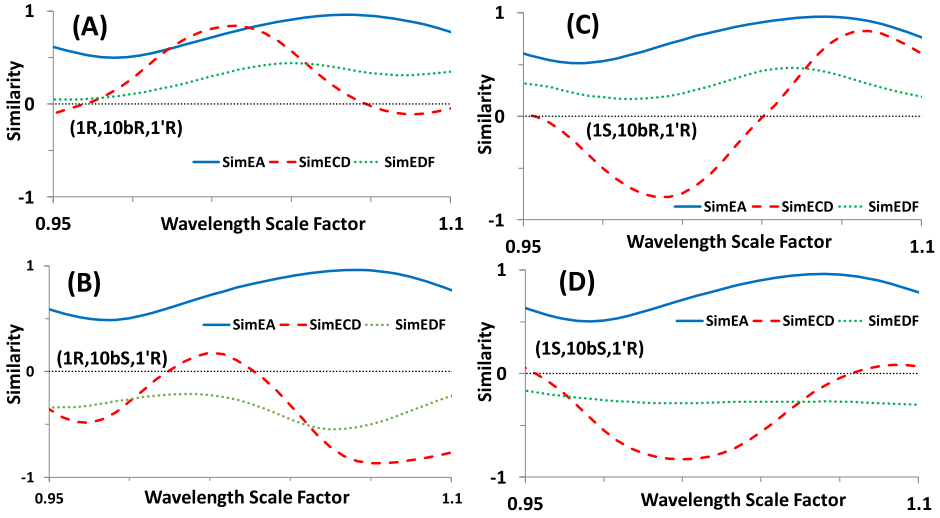

Figure 6. SSO plots comparing experimental EA, ECD, and EDF spectra with those predicted for four diastereomers at CAM-B3LYP/6-311++G(2d,2p)/PCM(methanol). (A) (1*R*,10*bR*,1′*R*), (B) (1*R*,10*bS*,1′*R*), (C) (1*S*,10*bR*,1′*R*), and (D) (1*S*,10*bS*,1′*R*). Inclusion of empirical D3 dispersion corrections did not influence these results.

transition associated with the predicted CEs are displayed in Figures S2−S4 of the SI.

The spectral similarity overlap (SSO) plots provide quantitative assessment of the agreement between experimental and predicted spectra. The maximum *Sim*EA, *Sim*ECD, and *Sim*EDF values seen for (1*R*,10*bR*,1′*R*) are 0.96, 0.84, and 0.45, respectively (Figure 6A). Ideally, these values should be close to 1 for perfect agreement, but *Sim*ECD, and *Sim*EDF values greater than ∼0.4, are considered necessary to reflect a reliable agreement between experiment and predictions. Therefore, a large *Sim*ECD value, and *Sim*EDF value greater than 0.4, provides further support for the conclusions derived from ORD analyses.

VCD of the (1R,10bR,1′R) Diastereomer. The experimental vibrational absorption (VA), VCD, and vibrational dissymmetry factor (VDF) spectra of **5** in the 1800−1160 cm^{-1} region are compared to the corresponding spectra predicted for the (1*R*,10*bR*,1′*R*) diastereomer, with deuterated OH groups, in Figure 7. In the left vertical panel of Figure 7, the predicted wavenumbers are scaled with 0.9815 (which corresponds to the maximum *Sim*VCD value) and overlaid on the experimental spectra. In the right vertical panel, predicted spectra with unscaled wavenumbers are stacked over

DOI: 10.1021/acsomega.8b03678
ACS Omega 2019, 4, 6154−6164

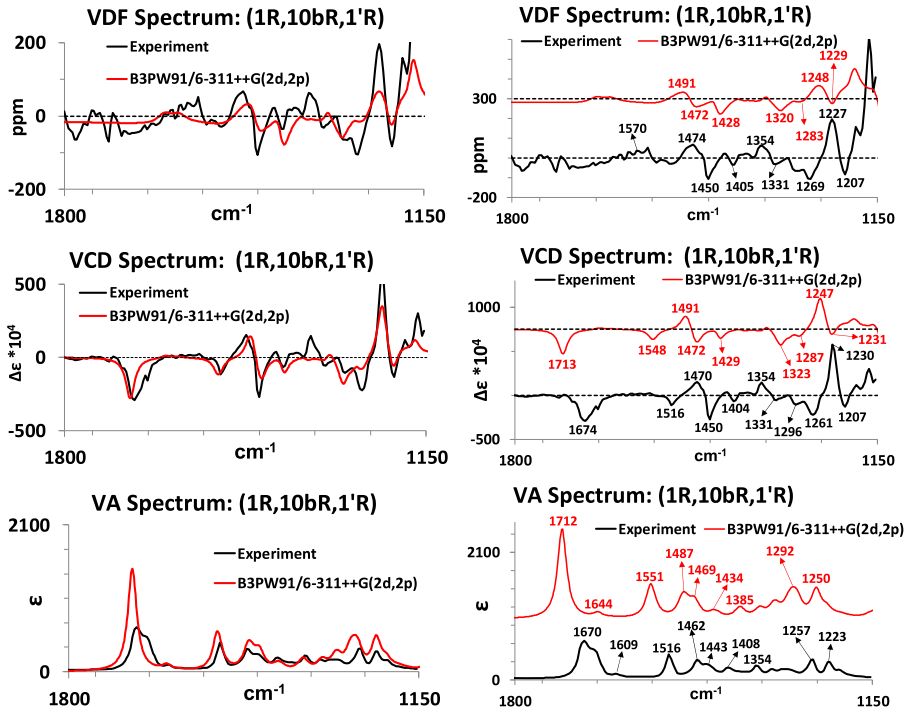

Figure 7. Comparison of experimental VA, VCD, and VDF spectra with those predicted for the (1*R*,10*bR*,1′*R*) diastereomer, with deuterated OH groups, at B3PW91/6-311++G(2d,2p)/PCM(methanol). In the left vertical panel, the predicted wavenumbers are scaled with 0.9815 (which corresponds to the maximum *Sim*VCD value) and overlaid on experimental spectra. In the right vertical panel, QC predicted spectra with unscaled wavenumbers are stacked over experimental spectra and band positions labeled.

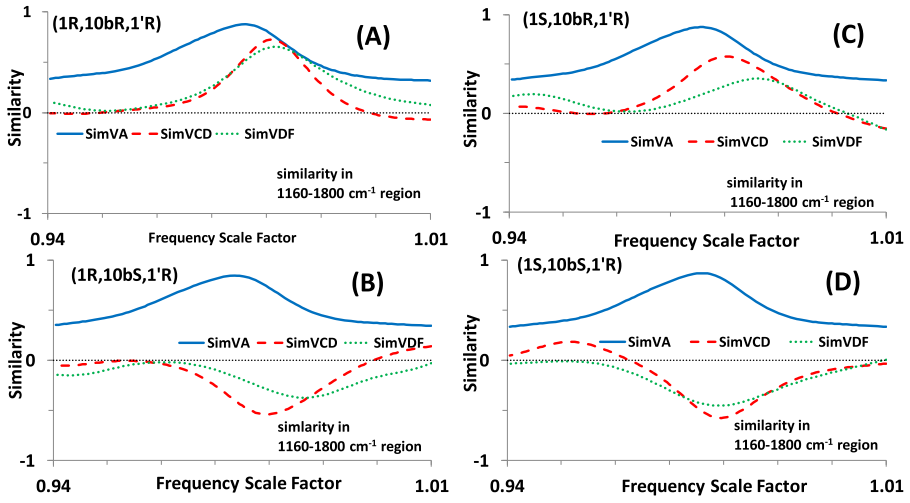

Figure 8. SSO plots comparing experimental VA, VCD, and VDF spectra with those predicted for four diastereomers, with deuterated OH groups, at B3PW91/6-311++G(2d,2p)/PCM(methanol). (A) (1*R*,10*bR*,1′*R*), (B) (1*R*,10*bS*,1′*R*), (C) (1*S*,10*bR*,1′*R*), and (D) (1*S*,10*bS*,1′*R*). Inclusion of empirical D3 dispersion corrections for the (1*R*,10*bR*,1′*R*) diastereomer resulted in lowered similarity measures; that for the (1*R*,10*bS*,1′*R*) diastereomer did not make significant changes to the data shown.

experimental spectra and band positions labeled. The correlations of experimental (and the corresponding unscaled predicted) VA band positions in cm^{-1} noted from the stacked spectra are as follows: 1670(1712), 1609(1644), 1516(1551), 1462(1487), 1443(1469), 1408(1434), 1354(1385), 1257(1292), and 1223(1250). Similarly, the correlations of experimental (and the corresponding unscaled predicted) VCD band positions in cm^{-1} are as follows: 1674(1713), 1516(1548), 1470(1491), 1450(1472), 1404(1429), 1296(1323), 1261(1287), 1230(1247), and 1207(1231). The positive experimental VCD band at 1354 cm^{-1} does not appear to have a corresponding positive predicted counterpart. This comparison indicates that most of the experimental bands are satisfactorily reproduced in the predicted spectra. Additionally, the relative intensities for all calculated VCD bands match those in the experimental spectrum.

It should be added that while experimental spectra are measured in the CD_3OD solvent where hydrogen bonding between the solute and solvent can take place, the predicted spectra used PCM, which does not account for solute−solvent hydrogen bonding. As a consequence, one may anticipate poorer agreement for some PCM predicted vibrational bands

DOI: 10.1021/acsomega.8b03678
ACS Omega 2019, 4, 6154−6164

in hydrogen-bonding solvents, leading to lower SSO values. Contrary to this anticipation, however, the agreement between experimental and predicted VCD spectra can be seen in Figure 7 to be excellent. The quantitative agreement between experimental and predicted spectra can be judged using maximum *Sim*VA, *Sim*VCD, and *Sim*VDF values in SSO plots. While *Sim*VA values are not useful for AC assignment, *Sim*VCD values, as well as *Sim*VDF values greater than or equal to ∼0.4,[39] are considered necessary to validate the agreement between experiment and predicted VCD spectra. The similarity analysis for the 1800−1160 cm^{-1} region yields maximum *Sim*VCD and *Sim*VDF values of 0.73 and 0.65, respectively, for (1*R*,10*bR*,1′*R*), as seen in Figure 8A. Such large values are normally encountered for small rigid molecules in non-hydrogen-bonding solvents and are uncommon for VCD spectra measured in the methanol-d_4 solvent. The quantitative agreement of experimental VCD and VDF spectra of **5** with those predicted for the (1*R*,10*bR*,1′*R*) diastereomer can therefore be considered excellent. Thus, the detailed analysis of the VCD spectra provides further support for the conclusions derived from ORD and ECD analyses.

The successful reproduction of experimental VCD spectra in the methanol-d_4 solvent by B3PW91/6-311++G(2d,2p) predictions, with PCM representing the hydrogen-bonding methanol solvent, can either be fortuitous or suggest one of the following two possibilities: (a) the intramolecular hydrogen-bonding network among the three O−H groups (see Figure 3) could be providing a stabilizing environment compared to intermolecular hydrogen bonding with solvent molecules or (b) the predicted spectra for **5** with intermolecular hydrogen bonding may not be significantly different from the ones obtained for **5** with intramolecular hydrogen bonding. These later assertions require the verification of the relative stability of, and spectral predictions for, solute conformers that are hydrogen bonded to methanol solvent molecules. One approach for determining the conformers that are hydrogen bonded to solvent molecules is to incorporate 1−3 explicit solvent molecules hydrogen bonded to one solute molecule and undertake theoretical predictions. However, such approaches lead to arbitrariness in the relative orientations of solvent molecules. Molecular dynamics (MD) simulations of the solute molecule embedded in a methanol solvent bath can provide a more reliable approach for this purpose. We hope to pursue the MD simulations in the near future.

The vibrational band assignments for the (1*R*,10*bR*,1′*R*) diastereomer derived from the animated vibrational motions in the GaussView program[40] are provided in Table S3 of the SI.

Chiroptical Spectroscopic Discrimination of Diastereomers. For chiral molecules with multiple stereocenters, it has become a common practice in the literature to predict chiroptical spectra for the relative configuration known from some other methods (such as single-crystal X-ray diffraction and/or NMR) and eliminate one of the two possible ACs using chiroptical spectroscopic methods. If the same practice is used here for **5**, and the information derived from X-ray data or the synthetic scheme is imposed as a constraint, then the AC of **5** could be correctly established using any one of the three chiroptical spectroscopic methods (ORD, ECD, or VCD). The relative configuration derived from X-ray data restricts the consideration of AC to either (1*R*,10*bR*,1′*R*) or (1*S*,10*bS*,1′*S*). ORD, ECD, and VCD analyses individually support the AC assignment as (1*R*,10*bR*,1′*R*) and do not support the AC assignment as (1*S*,10*bS*,1′*S*). The synthetic scheme fixes the ACs at 1 and 1′ positions to be (*R*), which restricts the consideration of AC of **5** to either (1*R*,10*bR*,1′*R*) or (1*R*,10*bS*,1′*R*). Again, ORD, ECD, and VCD analyses individually support the AC assignment as (1*R*,10*bR*,1′*R*) and do not support the AC assignment as (1*R*,10*bS*,1′*R*) (vide infra).

The validity of AC derived from chiroptical spectroscopic methods in this manner is subject to the validity of relative configuration that is started with. Therefore, diastereomer discrimination is an important objective for which recently developed microwave chiral detection methods are being pursued.[41,42] To ascertain if the chiroptical spectroscopic methods by themselves can provide enough diastereomer discrimination and determine the AC without depending on prior knowledge of relative configuration information, or of ACs at some of the stereogenic centers, one has to undertake QC predictions of chiroptical spectra for all possible diastereomers and evaluate if the correct diastereomer can be ascertained.[43−46] For this purpose, we have undertaken conformational analysis and QC predictions for all possible diastereomers. Due to the presence of three chiral centers, eight diastereomers are possible for **5**. Among these, four diastereomers are mirror images of the other four, so investigations are undertaken for four diastereomers: (1*R*,10*bR*,1′*R*), (1*R*,10*bS*,1′*R*), (1*S*,10*bR*,1′*R*), and (1*S*,10*bS*,1′*R*). The previous sections dealt with the (1*R*,10*bR*,1′*R*) diastereomer that is known to represent the correct AC for **5** (vide supra). Now we enquire if, in the absence of prior knowledge on the AC of **5**, the analyses of experimental and predicted ORD, ECD, and VCD data can determine the correct diastereomer.

The conformational analysis for the remaining diastereomers follows that used for (1*R*,10*bR*,1′*R*). The energies, populations, and ring puckering angles for conformers with a population of at least 1% are summarized in Table S4 of the SI. While (1*S*,10*bR*,1′*R*) and (1*S*,10*bS*,1′*R*) diastereomers have a single conformation with significantly higher populations than others, the (1*R*,10*bS*,1′*R*) diastereomer has three conformations with significantly higher populations than others.

The population-weighted ORD values predicted for these diastereomers are compared to the experimental ORD in Figure 4. It is seen that wavelength-dependent SORs of the (1*S*,10*bR*,1′*R*) diastereomer have the same signs and relatively closer magnitudes to those of experimental values, and therefore (1*S*,10*bR*,1′*R*) remains a viable candidate for assigning the AC of **5** based on ORD alone. For the (1*R*,10*bS*,1′*R*) and (1*S*,10*bS*,1′*R*) diastereomers, the signs of wavelength resolved SORs are opposite to those of experimental values, and the absolute magnitudes are comparable to the experimental magnitudes. Then, the antipodes of these diastereomers, namely, (1*S*,10*bR*,1′*S*) and (1*R*,10*bR*,1′*S*), remain viable candidates for assigning the AC of **5**. Thus, the criterion of matching the predicted ORD with the experimental ORD alone cannot be used as the sole criterion for assigning the unknown ACs of chiral molecules.[46]

The SSO plots of EA, ECD, and EDF spectra for (1*R*,10*bS*,1′*R*), (1*S*,10*bR*,1′*R*), and (1*S*,10*bS*,1′*R*) diastereomers are shown in Figure 6B−D, respectively, whereas individual comparisons of experimental and predicted EA and ECD spectra are provided in Figures S5−S7 of the SI. In the case of (1*S*,10*bR*,1′*R*), the SSO plot shows both positive and negative extremes of larger magnitudes for *Sim*ECD. Therefore, in principle, it becomes uncertain to decide whether this

DOI: 10.1021/acsomega.8b03678
ACS Omega 2019, 4, 6154−6164

diastereomer or its antipode matches the experimental spectra. However, the negative extreme occurs for a scale factor <1. Since predicted electronic transitions, at the theoretical level employed, generally occur at shorter wavelengths, a scale factor >1 is preferred, and therefore the positive extreme is considered for *Sim*ECD. The maximum SSO magnitudes for four diastereomers are summarized in Table 2. From the maximum SSO magnitudes in Table 2, it is seen that the (1*S*,10*bR*,1′*R*) diastereomer yields positive *Sim*ECD and *Sim*EDF values, whereas (1*R*,10*bS*,1′*R*) and (1*S*,10*bS*,1′*R*) diastereomers yield negative *Sim*ECD and *Sim*EDF values. The *Sim*EDF value for the (1*S*,10*bS*,1′*R*) diastereomer is not of sufficient magnitude to place reliance on the agreement. Thus, based on *Sim*ECD and *Sim*EDF values, (1*S*,10*bR*,1′*R*) and antipode of (1*R*,10*bS*,1′*R*) remain viable candidates for assigning the AC of **5**.

Table 2. SSO Values[a] of ECD, EDF, VCD, and VDF Spectra with Maximum Magnitudes

diastereomer	*Sim*ECD	*Sim*EDF	*Sim*VCD	*Sim*VDF
(1*R*, 10*bR*,1′*R*)[b]	0.84	0.45	0.73	0.65
(1*R*, 10*bS*,1′*R*)[c]	−0.87	−0.55	−0.54	−0.37
(1*S*, 10*bR*,1′*R*)[d]	0.82	0.47	0.58	0.35
(1*S*, 10*bS*,1′*R*)[e]	−0.82	−0.3	−0.58	−0.45

[a]1160−1800 cm^{-1} region used for VCD and VDF similarity overlap analyses. [b]Inclusion of empirical D3 dispersion correction gives the *Sim*ECD, *Sim*EDF, *Sim*VCD, and *Sim*VDF values as 0.84, 0.45, 0.67, and 0.63, respectively. [c]nclusion of empirical D3 dispersion correction gives the *Sim*ECD, *Sim*EDF, *Sim*VCD, and *Sim*VDF values as −0.9, −0.5, −0.57, and −0.39, respectively. [d]For this diasteromer, a large negative SSO also occurs for ECD at a scale factor of 1.01. But EDF remains positive; inclusion of empirical D3 dispersion correction gives the *Sim*ECD and *Sim*EDF values as 0.9 and 0.62, respectively. [e]*Sim*EDF remains approximately constant without a maximum in the SSO plot. This is an indication for unreliable conclusions; inclusion of empirical D3 dispersion correction gives the *Sim*ECD and *Sim*EDF values as −0.83 and −0.3, respectively.

The SSO plots of VA, VCD, and VDF spectra for (1*R*,10*bS*,1′*R*), (1*S*,10*bR*,1′*R*), and (1*S*,10*bS*,1′*R*) diastereomers are shown in Figure 8B−D, respectively, whereas individual comparisons of experimental and predicted VA and VCD spectra are provided in Figures S8−S10 of the SI. The maximum SSO magnitudes are summarized in Table 2. From Table 2, it is seen that the diastereomer (1*S*,10*bR*,1′*R*) yields maximum positive *Sim*VCD and *Sim*VDF values. The (1*R*,10*bS*,1′*R*) and (1*S*,10*bS*,1′*R*) diastereomers yield maximum negative *Sim*VCD and *Sim*VDF values. Based only on the magnitudes of *Sim*VCD, (1*R*,10*bS*,1′*R*), (1*S*,10*bR*,1′*R*), and (1*S*,10*bS*,1′*R*) diastereomers have large enough magnitudes to consider the (1*S*,10*bR*,1′*R*) diastereomer and the antipodes of (1*R*,10*bS*,1′*R*) and (1*S*,10*bS*,1′*R*) diastereomers as viable candidates for AC assignment. The magnitude of *Sim*VDF is also large enough to consider the antipode of (1*S*,10*bS*,1′*R*) as a viable candidate, but those for (1*R*,10*bS*,1′*R*) and (1*S*,10*bR*,1′*R*) diastereomers are close to ∼0.4. Therefore, the latter two would require further scrutiny for AC assignment.

It should be noted that the *Sim*VDF value depends on the experimental reliability criterion, that is, on the magnitudes of experimentally measured VCD signals that are considered reliable. If we consider that only the experimental VCD signals with Δ*A*/*A* greater than 10 ppm are reliable, then *Sim*VDF values for (1*R*,10*bS*,1′*R*) and (1*S*,10*bR*,1′*R*) diastereomers come out as −0.35 and 0.36, respectively (see Table S5 in the SI), and their magnitudes are still close to ∼0.4. But if we consider that only the experimental VCD signals with Δ*A*/*A* greater than 40 ppm are reliable (as has been recommended previously[47]), then *Sim*VDF values for (1*R*,10*bS*,1′*R*) and (1*S*,10*bR*,1′*R*) diastereomers drop to −0.23 and 0.16, respectively (see Table S5 in the SI), ruling out these two diastereomers as viable candidates. For the (1*S*,10*bS*,1′*R*) diastereomer, *Sim*VDF values are −0.46 and −0.44, respectively, for 10 ppm and 40 ppm criteria (see the Supporting Information), leaving its antipode in the consideration for assigning AC. Based on *Sim*VCD and *Sim*VDF values alone, the antipode of the (1*S*,10*bS*,1′*R*) diastereomer remains a viable candidate for assigning the AC of **5**.

Thus, ORD, ECD, and VCD analyses, independently, cannot provide a unique solution to the AC of **5**. A different situation emerges when we combine the results obtained from all three methods. Table 3 summarizes the conclusions derived from ORD comparisons and maximum SSO values derived from ECD and VCD spectral analyses. In this table, a "Y" entry indicates that the diastereomer belonging to that entry is a reliable candidate for the correct AC assignment; an "M" entry indicates that the antipode of the diastereomer belonging to that entry is a reliable candidate for correct AC; entries with "U" cast doubt on the reliability of AC assignment. The row belonging to (1*R*,10*bR*,1′*R*) has all Y entries, so the assignment of AC to this diastereomer is supported independently by ORD, ECD, EDF, VCD, and VDF. This is not the case for the other three rows. (1*S*,10*bR*,1′*R*) and the antipode of (1*R*,10*bS*,1′*R*) are not supported by the low magnitudes of VDF, whereas the antipode of the (1*S*,10*bS*,1′*R*) diastereomer is not supported by the low magnitude of EDF. However, when the conclusions from EDF and VDF analyses are combined, the (1*R*,10*bR*,1′*R*) diastereomer emerges as the single reliable candidate, which is also the AC determined from combined X-ray and synthetic analyses (vide supra).

Table 3. Possible Contenders[a] for AC of 5 as Deduced from ORD, ECD, EDF, VCD, and VDF Analyses

diastereomer	ORD	ECD	EDF	VCD	VDF
(1*R*,10*bR*,1′*R*)	Y	Y	Y	Y	Y
(1*R*,10*bS*,1′*R*)	M	M	M	M	U
(1*S*,10*bR*,1′*R*)	Y	Y	Y	Y	U
(1*S*,10*bS*,1′*R*)	M	M	U	M	M

[a]Y, possible contender; M, mirror image is a possible contender; U, uncertain.

It is important to note that if EDF and VDF are not included in Table 3 for assigning the AC of **5**, then four different diastereomers remain viable candidates, without offering diastereomer discrimination. Therefore, in the case of (−)-crispine A analogue investigated here, combined similarity analysis of EDF and VDF spectra turned out to be essential for determining the correct diastereomer.

For chiral molecules with multiple chiral centers, the situation encountered in the current work can occur more often than desired. To recognize new opportunities, and any limitations, chiroptical spectroscopic predictions should be undertaken for all possible diastereomers (regardless of the availability of prior knowledge on relative configurations), as recommended previously.[43−46]

DOI: 10.1021/acsomega.8b03678
ACS Omega 2019, 4, 6154−6164

CONCLUSIONS

An analogue of (−)-crispine A with three stereogenic centers has been synthesized and its AC established using the combined information derived from the synthetic scheme and single-crystal X-ray diffraction data. Either by constraining the relative configuration to be that derived from X-ray data or by constraining the ACs at two of the chiral centers to be those derived from the synthetic scheme, the AC of (−)-crispine A analogue can be correctly established using any one of the three chiroptical spectroscopic methods (ORD, ECD, or VCD). In the absence of such outside information, separate independent analysis of ORD, ECD, and VCD does not entail a unique solution to the AC, and multiple diastereomers present themselves as viable candidates for the AC of (−)-crispine A analogue. Combined EDF and VDF spectral analysis, however, rules out the incorrect diastereomers. Thus, the combined EDF and VDF spectral analysis is seen as a useful diastereomer discrimination tool.

METHODS

Experimental Section. *X-ray Crystallography.* Crystals of **5** were obtained from the saturated solution of the chloroform/hexane solvent system. The X-ray structure was obtained using a Bruker X8 KAPPA APEX II diffractometer using a wavelength of 0.71 Å.

ORD, ECD, and VCD Measurements. ORs were measured with an AutoPol IV automatic polarimeter at six discrete wavelengths (633, 589, 546, 436, 405, and 365 nm) at a concentration of 5.87 mg/mL in methanol solvent using a 0.5 dm quartz cell and converted to SORs by dividing the ORs with concentration (g/cm^3) and path length (dm). The experimental EA and ECD spectra were measured at 0.38 mg/mL in methanol solvent with an AVIV 215 ECD spectrometer using a 2 mm quartz cell. EA and ECD spectra were collected from 250 to 400 nm. Since absorbance at wavelengths shorter than 250 nm is too high, a lower concentration of 0.048 mg/mL in methanol solvent was used to collect EA and ECD spectra from 200 to 250 nm. These two sets of spectra were converted to epsilon units and merged smoothly at 250 nm without adjustments. The experimental VA and VCD spectra were measured with a ChiralIR VCD spectrometer at a concentration of 45 mg/mL in CD_3OD solvent using the SL3 cell with BaF_2 windows and 100 μm path length.

Spectral Similarity Overlap (SSO) Plots. SSO is calculated using the *Sim* function suggested by Shen et al.[48] This *Sim* function is written as[39]

$$Sim\mathrm{XXX}(\sigma) = \left(\int f_{\mathrm{XXX}}(\sigma{:}\ x)h_{\mathrm{XXX}}(x)\mathrm{d}x\right)\Big/\left(\int f_{\mathrm{XXX}}(\sigma{:}\ x)f_{\mathrm{XXX}}(\sigma{:}\ x)\mathrm{d}x + \int h_{\mathrm{XXX}}(x)h_{\mathrm{XXX}}(x)\mathrm{d}x - \left|\int f_{\mathrm{XXX}}(\sigma{:}\ x)h_{\mathrm{XXX}}(x)\mathrm{d}x\right|\right) \quad (1)$$

In eq 1, $h_{\mathrm{XXX}}(x)$ represents the experimental spectrum as a function of the running index for x-axis values; subscript XXX represents the type of spectrum (XXX = VA, VCD, VDF, EA, ECD, or EDF); f_{XXX} (σ:x) represents the simulated predicted spectrum obtained after scaling the predicted transition frequencies/wavelengths with a scale factor σ; *Sim*XXX (σ) represents the numerical measure of SSO between experimental and predicted spectra as a function of σ for the type of spectrum XXX; the integrals run over a continuous spectral region of interest. The display of *Sim*XXX (σ) as a function of σ is referred to as the SSO plot. For similarity analysis, VA, VCD, VDF, EA, ECD, and EDF spectra are normalized individually using square root of the sum of squared intensities.[49,50] The range for *Sim*ECD, *Sim*VCD, *Sim*EDF, and *Sim*VDF values is −1 to +1. A value of +1 indicates perfect agreement of experimental spectra with predicted spectra for the AC used in calculations. A value of −1 indicates perfect agreement of experimental spectra with predicted spectra for the AC opposite to the one used for calculations. The *Sim*VA and *Sim*EA values, which have a range of 0−1, do not relay any information on AC.

While separate evaluations of QC predictions of EA and ECD or VA and VCD spectral intensities may appear satisfactory, EDF and VDF (ratio of ECD/VCD to EA/VA) spectra are more challenging for QC predictions. For this purpose, we have advocated the quantitative analysis of experimental and predicted EDF and VDF spectra also for verifying the agreement between experimental and predicted ECD and VCD spectra.[39,47,51] The agreement between experimental and predicted spectra is quantified using maximum numerical values of *Sim*EA, *Sim*ECD, and *Sim*EDF for ECD spectra and *Sim*VA, *Sim*VCD, and *Sim*VDF values for VCD spectra in SSO plots. While *Sim*EA and *Sim*VA values come out to be generally high and not very discriminatory, *Sim*ECD and *Sim*EDF values for ECD, and *Sim*VCD and *Sim*VDF values for VCD, provide good measures of quantitative agreement between experimental observations and QC predictions. Achieving a *Sim*VCD value of +0.4 or higher is recommended for an acceptable agreement between experimental and calculated spectra for assigning the correct molecular structures.[39] Approximately the same value of *Sim*VDF is also recommended. The same criteria are used for *Sim*ECD and *Sim*EDF.

The errors in concentration and path length do not influence the EDF and VDF spectra when both absorption and CD spectra are measured simultaneously for the same sample and using the same instrument. The influences of baseline offsets and of CD magnitude calibration error are suppressed during the calculation of *Sim*EDF and *Sim*VDF by normalizing the intensities in DF spectra. This process can take care of the situations where the experimental baseline offset is constant as a function of wavenumber/wavelength and experimental CD magnitudes are off by a constant as a function of wavenumber/wavelength. If the CD baseline is not horizontal, then DF spectra cannot be used. For this reason, it is important to have a good-quality experimental CD spectrum with a horizontal baseline before proceeding to calculate the DF spectrum.

Calculation of DF spectra incorporates two features: (a) to help remove the amplification of noise in the regions where absorbance is nearly zero and the associated CD signal is only noise, a baseline tolerance value for absorption spectra is incorporated; and (b) the reliability level of experimental CD signals, determined by the experimental reliability criterion (previously referred to as the experimental robustness criterion[47]), based on the experimental $\Delta A/A$ values, is introduced. The choice for the experimental reliability criterion can vary from instrument to instrument and for individual research groups. For calculating the EDF spectra, we do not impose the experimental reliability criterion since ECD spectra generally have a good signal-to-noise ratio. The use of 40 ppm (i.e., $\Delta A/A = 4 \times 10^{-5}$) as the threshold for reliability results in blanking out the spectral regions with VDF less than 40 ppm, leading to spectral discontinuities in the VDF spectra. To avoid the spectral discontinuities, the VDF spectral analysis

DOI: 10.1021/acsomega.8b03678
ACS Omega 2019, 4, 6154−6164

presented in this manuscript did not impose any experimental reliability criterion. Nevertheless, we calculated the VDF spectra with experimental reliability criteria of 10 ppm and 40 ppm, and the resulting *Sim*VDF values are presented in Figure S5 of the SI.

■ ASSOCIATED CONTENT

Supporting Information

The Supporting Information is available free of charge on the ACS Publications website at DOI: 10.1021/acsomega.8b03678.

> Crystal structure parameters, bond lengths and angles, conformer specific EA and ECD spectra, highest occupied molecular orbital−lowest occupied molecular orbital diagrams, vibrational assignments, Gibbs energies and populations for conformers of diastereomers, EA/ECD/EDF and VA/VCD/VDF spectra for diastereomers, VDF values as a function of experimental reliability criterion (PDF)

■ AUTHOR INFORMATION

Corresponding Authors

*E-mail: (I.I.) i.ibnusaud@gmail.com.
*E-mail: (P.L.P.) Prasad.L.Polavarapu@Vanderbilt.Edu.

ORCID

Prasad L. Polavarapu: 0000-0001-6458-0508

Notes

The authors declare no competing financial interest.

■ ACKNOWLEDGMENTS

We thank Professor David W. Wright for allowing us to use his ECD instrument, Dr. Vijay Raghavan for assistance with VCD and ORD measurements, Dr. Ernesto Santoro for help with identifying electronic transitions, and Mr. Lee S. Cantrell for participating in the initial stages of calculations. P.L.P. acknowledges funding from National Science Foundation (CHE-1464874) and II acknowledges funding from DST, Govt. of India (project No. SR/S1/OC-98/2012). This work was conducted in part using the resources of the Advanced Computing Center for Research and Education (ACCRE) at Vanderbilt University.

■ REFERENCES

(1) Kapat, A.; Kumar, P. S.; Baskaran, S. Synthesis of crispine A analogues via an intramolecular Schmidt reaction. *Beilstein J. Org. Chem.* **2007**, *3*, 49 DOI: 10.1186/1860-5397-3-49.

(2) King, F. D. A facile three-step synthesis of (±)-crispine A via an acyliminium ion cyclisation. *Tetrahedron* **2007**, *63*, 2053−2056.

(3) Bailey, K. R.; Ellis, A. J.; Reiss, R.; Snape, T. J.; Turner, N. J. A template-based mnemonic for monoamine oxidase (MAO-N) catalyzed reactions and its application to the chemo-enzymatic deracemisation of the alkaloid (±)-crispine A. *Chem. Commun.* **2007**, *35*, 3640−3642.

(4) Szawkało, J.; Zawadzka, A.; Wojtasiewicz, K.; Leniewski, A.; Drabowicz, J.; Czarnocki, Z. First enantioselective synthesis of the antitumour alkaloid (+)-crispine A and determination of its enantiomeric purity by 1H NMR. *Tetrahedron: Asymmetry* **2005**, *16*, 3619−3621.

(5) Knölker, H.-J.; Agarwal, S. Total synthesis of the antitumor active pyrrolo[2,1-a]isoquinoline alkaloid (±)-crispine A. *Tetrahedron Lett.* **2005**, *46*, 1173−1175.

(6) Kumar, P. S.; Kapat, A.; Baskaran, S. An intramolecular Schmidt reaction strategy for the synthesis of a methyl analogue of crispine A. *Tetrahedron Lett.* **2008**, *49*, 1241−1243.

(7) Prasanth, C. P.; Joseph, E.; Abhijith, A.; Nair, D. S.; Ibnusaud, I.; Raskatov, J.; Singaram, B. Stabilization of NaBH4 in Methanol Using a Catalytic Amount of NaOMe. Reduction of Esters and Lactones at Room Temperature without Solvent-Induced Loss of Hydride. *J. Org. Chem.* **2018**, *83*, 1431−1440.

(8) Zhang, Q.; Tu, G.; Zhao, Y.; Cheng, T. Novel bioactive isoquinoline alkaloids from *Carduus crispus*. *Tetrahedron* **2002**, *58*, 6795−6798.

(9) Yuste, F.; Sánchez-Obregón, R.; Díaz, E.; García-Carrillo, M. A. Enantiodifferentiation of the antitumor alkaloid crispine A using the NMR chiral solvating agents (R)- and (S)-BINOL. *Tetrahedron: Asymmetry* **2014**, *25*, 224−228.

(10) Nicolaou, K. C.; Snyder, S. A. Chasing Molecules That Were Never There: Misassigned Natural Products and the Role of Chemical Synthesis in Modern Structure Elucidation. *Angew. Chem., Int. Ed.* **2005**, *44*, 1012−1044.

(11) Maier, M. E. Structural revisions of natural products by total synthesis. *Nat. Prod. Rep.* **2009**, *26*, 1105−1124.

(12) Suyama, T. L.; Gerwick, W. H.; McPhail, K. L. Survey of marine natural product structure revisions: A synergy of spectroscopy and chemical synthesis. *Bioorg. Med. Chem.* **2011**, *19*, 6675−6701.

(13) Polavarapu, P. L., *Chiroptical Spectroscopy: Fundamentals and Applications*. CRC Press: Boca Raton, FL, 2016.

(14) Berova, N.; Polavarapu, P. L.; Nakamishi, K.; Woody, R. W. *Comprehensive Chiroptical Spectroscopy*; Wiley: New York, 2012; Vol. *1*−*2*.

(15) Lowry, T. M. *Optical Rotatory Power*; Dover Publications: New York, 1964.

(16) Pescitelli, G.; Di Bari, L.; Berova, N. Application of electronic circular dichroism in the study of supramolecular systems. *Chem. Soc. Rev.* **2014**, *43*, 5211−5233.

(17) Nafie, L. A.; Dukor, R. K. Vibrational Optical Activity in Chiral Analysis. In *Chiral Analysis*, 2nd ed.; Polavarapu, P. L., Ed.; Elsevier, 2018; Chapter 5, pp 201−247.

(18) Ostovar pour, S.; Barron, L. D.; Mutter, S. T.; Blanch, E. W. Raman Optical Activity. In *Chiral Analysis*, 2nd ed.; Polavarapu, P. L., Ed.; Elsevier, 2018; Chapter 6, pp 249−291.

(19) Polavarapu, P. L. Why is it important to simultaneously use more than one chiroptical spectroscopic method for determining the structures of chiral molecules? *Chirality* **2008**, *20*, 664−672.

(20) Buckingham, A. D.; Fowler, P. W.; Galwas, P. A. Velocity-Dependent Property Surfaces and the Theory of Vibrational Circular Dichroism. *Chem. Phys.* **1987**, *112*, 1−14.

(21) Galwas, P. A. On the Distribution of Optical Polarization in Molecules. Ph.D. Thesis, Cambridge University: Cambridge, 1983.

(22) Stephens, P. J. Theory of Vibrational Circular Dichroism. *J. Phys. Chem.* **1985**, *89*, 748−752.

(23) Frisch, M. J.; Trucks, G. W.; Schlegel, H. B.; Scuseria, G. E.; Robb, M. A.; Cheeseman, J. R.; Scalmani, G.; Barone, V.; Mennucci, B.; Petersson, G. A.; Nakatsuji, H.; Caricato, M.; Li, X.; Hratchian, H. P.; Izmaylov, A. F.; Bloino, J.; Zheng, G.; Sonnenberg, J. L.; Hada, M.; Ehara, M.; Toyota, K.; Fukuda, R.; Hasegawa, J.; Ishida, M.; Nakajima, T.; Honda, Y.; Kitao, O.; Nakai, H.; Vreven, T.; Montgomery, J. J. A. *Gaussian 09*, revision D; Gaussian Inc.: Wallingford, CT, 2009.

(24) DALTON:A Molecular Electronic Structure Program. http://daltonprogram.org, 2015.

(25) PSI4: A Open-Source Suite of Ab Initio Quantum Chemistry Programs. www.psicode.org/, 2014.

(26) Padwa, A.; Heidelbaugh, T. M.; Kuethe, J. T.; McClure, M. S. Heterocyclic Synthesis via the Tandem Thionium/N-Acyliminium Ion Cascade. *J. Org. Chem.* **1998**, *63*, 6778−6779.

(27) Luker, T.; Koot, W.-J.; Hiemstra, H.; Speckamp, W. N. Michael Additions to (R)-1-Acetyl-5-isopropoxy-3-pyrrolin-2-one and Subsequent N-Acyliminium Ion Generation: Synthesis of Enantiopure 1-

DOI: 10.1021/acsomega.8b03678
ACS Omega 2019, 4, 6154−6164

Azabicycles and Preparation of an Intermediate for a Projected Synthesis of Roseophilin. *J. Org. Chem.* **1998**, *63*, 220−221.
(28) Wijnberg, B. P.; Speckamp, W. N. Diastereoselective cyclisations of chiral α-acyliminium ions. *Tetrahedron Lett.* **1980**, *21*, 1987−1990.
(29) Prelog, V.; Helmchen, G. Basic Principles of the CIP-System and Proposals for a Revision. *Angew. Chem., Int. Ed.* **1982**, *21*, 567−583.
(30) Conflex: High Performance Conformational Analysis. www.conflex.net. May 23, 2018.
(31) Becke, A. D. Density-functional thermochemistry. III. The role of exact exchange. *J. Chem. Phys.* **1993**, *98*, 5648−5652.
(32) Lee, C.; Yang, W.; Parr, R. G. Development of the Colle-Salvetti correlation-energy formula into a functional of the electron density. *Phys. Rev. B* **1988**, *37*, 785−789.
(33) Vosko, S. H.; Wilk, L.; Nusair, M. Accurate spin-dependent electron liquid correlation energies for local spin density calculations: a critical analysis. *Can. J. Phys.* **1980**, *58*, 1200−1211.
(34) Hehre, W. J.; Radom, L.; Schleyer, P. v.R.; Pople, J. A. *Ab Initio Molecular Orbital Theory*; John Wiley: New York, 1986.
(35) Frisch, M. J.; Trucks, G. W.; Schlegel, H. B.; Scuseria, G. E.; Robb, M. A.; Cheeseman, J. R.; Scalmani, G.; Barone, V.; Mennucci, B.; Petersson, G. A.; Nakatsuji, H.; Caricato, M.; Li, X.; Hratchian, H. P.; Izmaylov, A. F.; Bloino, J.; Zheng, G.; Sonnenberg, J. L.; Hada, M.; Ehara, M.; Toyota, K.; Fukuda, R.; Hasegawa, J.; Ishida, M.; Nakajima, T.; Honda, Y.; Kitao, O.; Nakai, H.; Vreven, T.; Montgomery, J. A.; Peralta, J. E.; Ogliaro, F.; Bearpark, M.; Heyd, J. J.; Brothers, E.; Kudin, K. N.; Staroverov, V. N.; Kobayashi, R.; Normand, J.; Raghavachari, K.; Rendell, A.; Burant, J. C.; Iyengar, S. S.; Tomasi, J.; Cossi, M.; Rega, N.; Millam, J. M.; Klene, M.; Knox, J. E.; Cross, J. B.; Bakken, V.; Adamo, C.; Jaramillo, J.; Gomperts, R.; Stratmann, R. E.; Yazyev, O.; Austin, A. J.; Cammi, R.; Pomelli, C.; Ochterski, J. W.; Martin, R. L.; Morokuma, K.; Zakrzewski, V. G.; Voth, G. A.; Salvador, P.; Dannenberg, J. J.; Dapprich, S.; Daniels, A. D.; Farkas, Ö.; Foresman, J. B.; Ortiz, J. V.; Cioslowski, J.; Fox, D. J. *Gaussian 09*, revision D; Gaussian Inc.: Wallingford, CT, 2009.
(36) Scalmani, G.; Frisch, M. J. Continuous surface charge polarizable continuum models of solvation. I. General formalism. *J. Chem. Phys.* **2010**, *132*, No. 114110.
(37) Yanai, T.; Tew, D. P.; Handy, N. C. A new hybrid exchange−correlation functional using the Coulomb-attenuating method (CAM-B3LYP). *Chem. Phys. Lett.* **2004**, *393*, 51−57.
(38) Grimme, S.; Antony, J.; Ehrlich, S.; Krieg, H. A consistent and accurate ab initio parametrization of density functional dispersion correction (DFT-D) for the 94 elements H-Pu. *J. Chem. Phys.* **2010**, *132*, No. 154104.
(39) Polavarapu, P. L.; Covington, C. L.; Raghavan, V. To Avoid Chasing Incorrect Chemical Structures of Chiral Compounds: Raman Optical Activity and Vibrational Circular Dichroism Spectroscopies. *ChemPhysChem* **2017**, *18*, 2459−2465.
(40) *Gaussview*, version 5. Gaussian Inc: Willingford, CT, 2004.
(41) Domingos, S. R.; Pérez, C.; Schnell, M. Sensing Chirality with Rotational Spectroscopy. *Annu. Rev. Phys. Chem.* **2018**, *69*, 499−519.
(42) Pate, B. H.; Evangelisti, L.; Caminati, W.; Xu, Y.; Thomas, J.; Patterson, D.; Perez, C.; Schnell, M. Quantitative Chiral Analysis by Molecular Rotational Spectroscopy. In *Chiral Analysis*, 2nd ed.; Polavarapu, P. L., Ed.; Elsevier, 2018; Chapter 17, pp 679−729.
(43) Polavarapu, P. L. Molecular Structure Determination Using Chiroptical Spectroscopy: Where We May Go Wrong? *Chirality* **2012**, *24*, 909−920.
(44) Polavarapu, P. L.; Donahue, E. A.; Shanmugam, G.; Scalmani, G.; Hawkins, E. K.; Rizzo, C.; Ibnusaud, I.; Thomas, G.; Habel, D.; Sebastian, D. A Single Chiroptical Spectroscopic Method May Not Be Able To Establish the Absolute Configurations of Diastereomers: Dimethylesters of Hibiscus and Garcinia Acids. *J. Phys. Chem. A* **2011**, *115*, 5665−5673.
(45) Polavarapu, P. L. Determination of the structures of chiral natural products using vibrational circular dichroism. In *Comprehensive Chiroptical spectroscopy*; Berova, N.; Polavarapu, P. L.; Nakanishi, K.; Woody, R. W., Eds.; John Wiley & sons: Hoboken, 2012; Vol. 2.
(46) Johnson, J. L.; Raghavan, V.; Cimmino, A.; Moeini, A.; Petrovic, A. G.; Santoro, E.; Superchi, S.; Berova, N.; Evidente, A.; Polavarapu, P. L. Absolute configurations of chiral molecules with multiple stereogenic centers without prior knowledge of the relative configurations: A case study of inuloxin C. *Chirality* **2018**, *30*, 1206−1214.
(47) Covington, C.; Polavarapu, P. Similarity in Dissymmetry Factor Spectra: A Quantitative Measure of Comparison between Experimental and Predicted Vibrational Circular Dichroism. *J. Phys. Chem. A* **2013**, *117*, 3377−3386.
(48) Shen, J.; Zhu, C.; Reiling, S.; Vaz, R. A novel computational method for comparing vibrational circular dichroism spectra. *Spectrochim. Acta, Part A* **2010**, *76*, 418−422.
(49) Covington, C. L.; Polavarapu, P. L. CDSpecTech: A single software suite for multiple chiroptical spectroscopic analyses. *Chirality* **2017**, *29*, 178−192.
(50) Covington, C.; Polavarapu, P. L. CDSpecTech: Computer programs for calculating similarity measures of comparison between experimental and calculated dissymmetry factors and circular intensity differentials, 22. https://sites.google.com/site/cdspectech1/, 2016.
(51) Junior, F. M.; Covington, C. L.; de Amorim, M. B.; Velozo, L. S.; Kaplan, M. A.; Polavarapu, P. L. Absolute Configuration of a Rare Sesquiterpene: (+)-3-Ishwarone. *J. Nat. Prod.* **2014**, *77*, 1881−1886.

DOI: 10.1021/acsomega.8b03678
ACS Omega 2019, 4, 6154−6164